The Journal of Neuroscience, December 1, 1998, *18*(23):9607–9619

Slow Closed-State Inactivation: A Novel Mechanism Underlying Ramp Currents in Cells Expressing the hNE/PN1 Sodium Channel

Theodore R. Cummins,[1,3] **James R. Howe,**[2] **and Stephen G. Waxman**[1,2,3]

Departments of [1]*Neurology and* [2]*Pharmacology, Yale University School of Medicine, New Haven, Connecticut 06510, and* [3]*Neuroscience Research Center, Veterans Administration Medical Center, West Haven, Connecticut 06516*

To better understand why sensory neurons express voltage-gated Na^+ channel isoforms that are different from those expressed in other types of excitable cells, we compared the properties of the hNE sodium channel [a human homolog of PN1, which is selectively expressed in dorsal root ganglion (DRG) neurons] with that of the skeletal muscle Na^+ channel (hSkM1) [both expressed in human embryonic kidney (HEK293) cells]. Although the voltage dependence of activation was similar, the inactivation properties were different. The $V_{1/2}$ for steady-state inactivation was slightly more negative, and the rate of open-state inactivation was ~50% slower for hNE. However, the greatest difference was that closed-state inactivation and recovery from inactivation were up to fivefold slower for hNE than for hSkM1 channels. TTX-sensitive (TTX-S) currents in small DRG neurons also have slow closed-state inactivation, suggesting that hNE/PN1 contributes to this TTX-S current. Slow ramp depolarizations (0.25 mV/msec) elicited TTX-S persistent currents in cells expressing hNE channels, and in DRG neurons, but not in cells expressing hSkM1 channels. We propose that slow closed-state inactivation underlies these ramp currents. This conclusion is supported by data showing that divalent cations such as Cd^{2+} and Zn^{2+} (50–200 μM) slowed closed-state inactivation and also dramatically increased the ramp currents for DRG TTX-S currents and hNE channels but not for hSkM1 channels. The hNE and DRG TTX-S ramp currents activated near −65 mV and therefore could play an important role in boosting stimulus depolarizations in sensory neurons. These results suggest that differences in the kinetics of closed-state inactivation may confer distinct integrative properties on different Na^+ channel isoforms.

Key words: sodium channel; persistent current; dorsal root ganglion; excitability; tetrodotoxin; expression

One of the hallmarks of most excitable cells is the presence of voltage-gated sodium currents, which underlie the rapid action potentials characteristic of neurons and muscle cells. Nearly a dozen distinct voltage-gated sodium channels have been cloned from mammals (Black and Waxman, 1996). Many of these channels have specific developmental, tissue, or cellular distributions. Rat brain type III neuronal channels are primarily expressed early during development (Felts et al., 1997). Immunocytochemical experiments indicate that although rat brain type I (rbI) channels are concentrated in cell bodies, rat brain type II (rbII) channels may be preferentially targeted to neurites (Westenbroek et al., 1989). Other neuronal isoforms are predominantly expressed in peripheral tissues (Akopian et al., 1996; Felts et al., 1997; Toledo-Aral et al., 1997; Dib-Hajj et al., 1998).

It is becoming apparent that the different isoforms may also have distinct functional properties. For example, Smith and Goldin (1998) have shown that although rbI and rbII channels both encode fast sodium currents, the voltage dependence of activation and steady-state inactivation is significantly more positive for the rbI channels. Recent evidence indicates that the Na6 isoform underlies resurgent and subthreshold persistent sodium currents in cerebellar Purkinje cells (Raman and Bean, 1997). One of the isoforms primarily expressed in peripheral neurons such as dorsal root ganglion (DRG) neurons, SNS or PN3, encodes a TTX-resistant channel that has slow inactivation kinetics when expressed in *Xenopus* oocytes (Akopian et al., 1996; Sangameswaran et al., 1996). Another isoform that is also highly expressed in DRG neurons (hNE, NaS, or PN1) has been cloned from human (Klugbauer et al., 1995), rabbit (Belcher et al., 1995) and rat (Sangameswaran et al., 1997; Toledo-Aral et al., 1997) and encodes a TTX-sensitive (TTX-S) channel (Klugbauer et al., 1995).

The human homolog of this isoform, hNE, has been expressed in the mammalian human embryonic kidney cell line HEK293, but the initial characterization did not demonstrate any exceptional differences between hNE and other TTX-S isoforms (Klugbauer et al., 1995). This isoform is particularly interesting because it is expressed in a majority of small DRG neurons (Black et al., 1996) and may be the predominant TTX-S channel in these sensory neurons. We (Cummins and Waxman, 1997) and others (Elliott and Elliott, 1993) have shown that the predominant TTX-S current in small DRG neurons from adult rats has slow repriming (recovery from inactivation) kinetics, much slower than those observed in adult CNS neurons (Costa, 1996) and axotomized DRG neurons (Cummins and Waxman, 1997). Therefore we were interested in determining whether the hNE sodium channel had slow repriming kinetics or other unique properties.

MATERIALS AND METHODS

Transfection and preparation of stably transfected cell lines. Transfections were performed using the calcium phosphate precipitation technique. HEK293 cells are grown under standard tissue culture conditions (5% CO_2; 37°C) in DMEM supplemented with 10% fetal bovine serum. The

Received June 23, 1998; revised Sept. 11, 1998; accepted Sept. 11, 1998.

This work was supported in part by the Medical Research Service, Department of Veterans Affairs, and by a grant from the National Multiple Sclerosis Society. T.R.C. was supported in part by a fellowship from the Paralyzed Veterans of America Spinal Cord Research Foundation.

Correspondence should be addressed to Dr. Stephen G. Waxman, Department of Neurology, LCI 707, Yale University School of Medicine, 333 Cedar Street, New Haven, CT 06510.

 0270-6474/98/189607-13$05.00/0

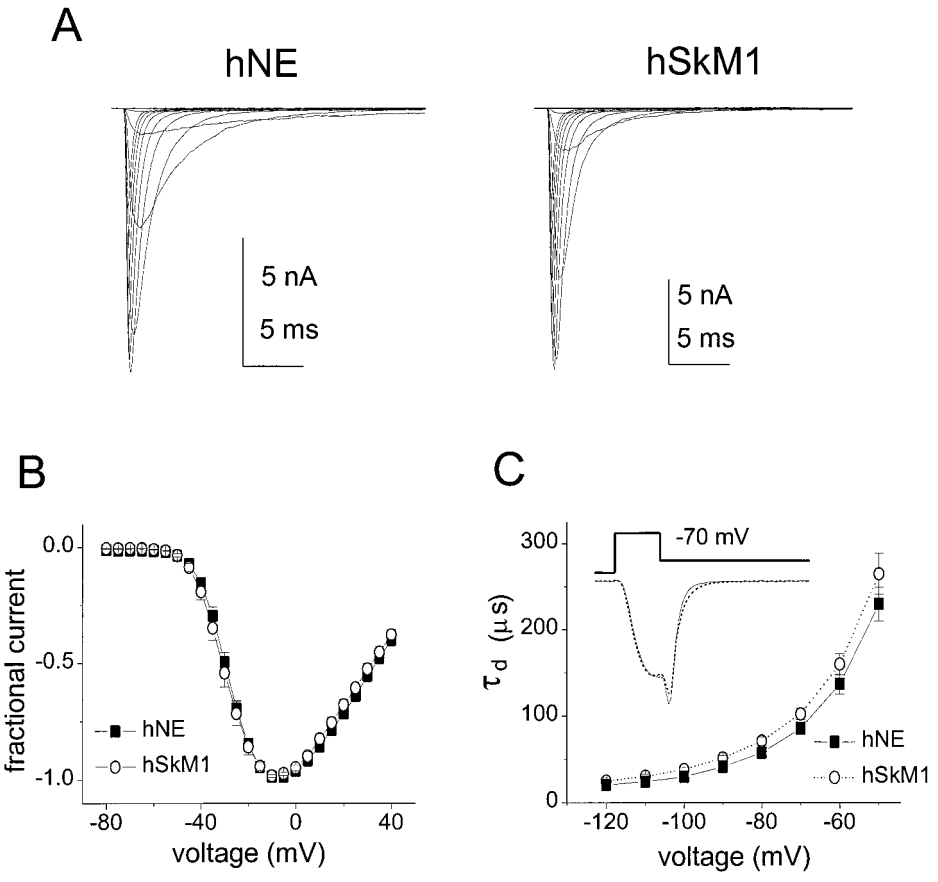

Figure 1. hNE and hSkM1 channels have similar activation properties. *A*, Family of *traces* from representative HEK293 cells expressing either hNE channels (*left*) or hSkM1 channels (*right*). The currents were elicited by 40 msec test pulses to various potentials from −60 to 30 mV. Cells were held at −100 mV. *B*, Normalized peak current–voltage relationship for hNE (*filled squares*; $n = 14$) and hSkM1 (*open circles*; $n = 12$). *C*, The deactivation time course of hNE and hSkM1 channels examined at potentials ranging from −120 to −50 mV after a 0.5 msec activation prepulse to 0 mV. Deactivation time constants were obtained from single-exponential fits to the tail currents for hNE (*filled squares*; $n = 16$) or hSkM1 (*open circles*; $n = 12$) channels. *Inset*. *Traces* showing representative hNE (*solid line*) and hSkM1 (*dotted line*) deactivation tail currents at −70 mV.

calcium phosphate–DNA mixture was added to the cell culture medium and left for 15–20 hr, after which time the cells were washed with fresh medium. After 48 hr, antibiotic (G418, Geneticin; Life Technologies, Gaithersburg, MD) was added to select for neomycin-resistant cells. After 2–3 weeks in G418, colonies were picked, split, and subsequently tested for channel expression using whole-cell patch-clamp recording techniques.

Culture of dorsal root ganglion neurons. DRG cells were studied after short-term culture (12–24 hr). The culture was performed as previously described (Caffrey et al., 1992). Briefly, the L4 and L5 DRG ganglia were harvested from adult female Sprague Dawley rats. The DRG were treated with collagenase and papain, dissociated in DMEM and Ham's F12 medium supplemented with 10% fetal bovine serum, and plated on glass coverslips. Recordings were made within 24 hr of dissociation.

Whole-cell patch-clamp recordings. Whole-cell patch-clamp recordings were conducted at room temperature (~21°C) using an EPC-9 amplifier. Data were acquired on a Macintosh Quadra 950 computer using the Pulse program (version 7.89; HEKA Electronic). Fire-polished electrodes (0.8–1.5 MΩ) were fabricated from 1.65 mm Corning 7052 capillary glass using a Sutter P-97 puller (Novato, CA). To minimize space-clamp problems, we selected for recording only isolated cells with a soma diameter of <25 μm. Cells were not considered for analysis if the initial seal resistance was <5 GΩ or if they had high leakage currents (holding current > 0.1 nA at −80 mV), membrane blebs, or an access resistance >4 MΩ. The average access resistance was 2.3 ± 0.6 MΩ (mean ± SD; $n = 116$) for cells expressing hNE channels and 2.3 ± 0.6 MΩ ($n = 52$) for cells expressing hSkM1 channels. Voltage errors were minimized using 80% series resistance compensation, and the capacitance artifact was canceled using the computer-controlled circuitry of the patch-clamp amplifier. Linear leak subtraction, based on resistance estimates from four to five hyperpolarizing pulses applied before the depolarizing test potential, was used for all voltage-clamp recordings. Membrane currents were usually filtered at 2.5 kHz and sampled at 10 kHz. The pipette solution contained (in mM): 140 CsF, 1 EGTA, 10 NaCl, and 10 HEPES, pH 7.3. The standard bathing solution was (in mM): 140 NaCl, 3 KCl, 1 $MgCl_2$, 1 $CaCl_2$, and 10 HEPES, pH 7.3. The liquid junction potential for these solutions was <8 mV; data were not corrected to account for this offset. The osmolarity of all solutions was adjusted to 310 mOsm (Wescor 5500 osmometer, Logan, UT). The offset potential was zeroed before patching the cells and checked after each recording for drift; if the drift was >10 mV per hour, the recording was discarded.

Data analysis. Data were analyzed using the Pulsefit (HEKA Electronic) and Origin (Microcal Software, Northampton, MA) software programs. Unless otherwise noted, statistical significance was determined by $p < 0.05$ using an unpaired t test. Results are presented as mean ± SEM, and error bars in the figures represent SEs. The curves in the figures are drawn to guide the eye unless otherwise noted. Time course data were fitted with single-exponential functions. Although in some instances fitting to a dual exponential would improve the overall fit, the second component was typically small (<10%), and the predominant component was not much different from that estimated with the single-exponential fits.

RESULTS

Sodium current activation

To compare the properties of the hNE (Klugbauer et al., 1995) and hSkM1 (George et al., 1992) sodium channels, we created HEK293 cell lines that stably expressed the hNE and hSkM1 channels. Fast-inactivating TTX-S sodium currents were observed in cells transfected with hNE and hSkM1 channels (Fig. 1*A*). Figure 1*B* shows that the current–voltage (*I–V*) curve for the peak sodium current was similar for hNE and hSkM1 channels. The midpoint of activation was −25.8 ± 0.8 mV (mean ± SE; $n = 45$) for hNE currents and −27.0 ± 0.8 mV ($n = 31$) for hSkM1 currents.

Other parameters relating to activation were also examined. The time course of activation, estimated using a Hodgkin and Huxley fit of currents elicited with a step depolarization to −30 mV, was similar for hNE channels ($\tau_m = 303 \pm 17$ μsec; $n = 25$) and hSkM1 channels ($\tau_m = 289 \pm 23$ μsec; $n = 20$). Deactivation

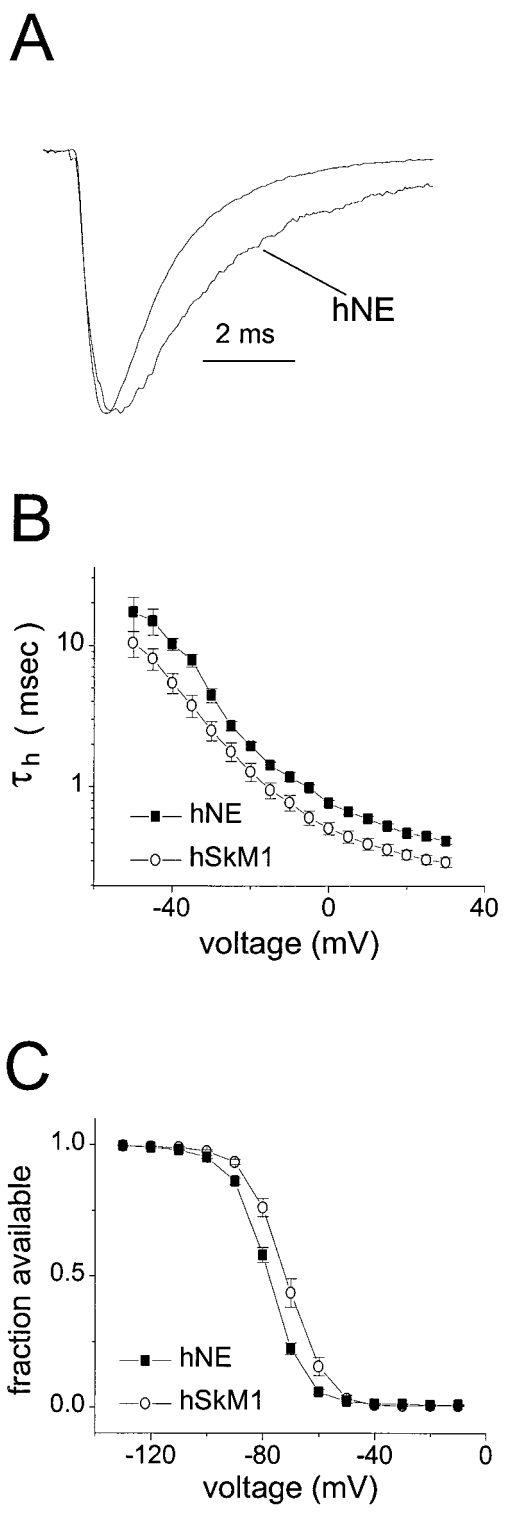

Figure 2. hNE and hSkM1 channels have distinct inactivation properties. *A*, Representative currents from whole-cell recordings of a cell expressing hNE channels (*trace* labeled *hNE*) and a cell expressing hSkM1 channels (*unlabeled trace*). Currents were elicited by a step depolarization to −30 mV from a holding potential of −100 mV and were scaled for comparison. The hNE current decays more slowly than does the hSkM1 current. *B*, Inactivation kinetics as a function of voltage. The macroscopic decay time constant is greater for hNE currents (*filled squares*; $n = 10$) than for hSkM1 currents (*open circles*; $n = 10$) at each voltage. Time constants were estimated from single-exponential fits to the decay phase of currents elicited by 100 msec step depolarizations to the indicated potential. *C*, Comparison of hNE (*filled squares*; $n = 13$) and hSkM1 (*open circles*; $n = 12$) steady-state inactivation. Steady-state inactivation was estimated by measuring the peak current amplitude elicited by 20 msec test pulses to −10 mV after 500 msec prepulses to potentials over the range of −130 to −10 mV. Current is plotted as a fraction of the maximum peak current.

kinetics was examined at potentials ranging from −120 to −50 mV after a short (0.5 msec) activating pulse (see Fig. 1*C*, *current traces*). Figure 1*C* shows that the time constants for deactivation were also similar for hNE and hSkM1 channels. Resurgent currents such as those reported by Raman et al. (1997) in Purkinje neurons were not observed in HEK293 cells expressing either hNE or hSkM1 channels. Noninactivating currents, defined as the residual current measured at 100 msec during a step depolarization to 0 mV, were small for both hNE channels (0.1 ± 0.1% of peak; $n = 23$) and hSkM1 channels (0.1 ± 0.1% of peak; $n = 17$).

Steady-state inactivation and inactivation kinetics

Although the activation kinetics is similar for hNE and hSkM1 currents, Figure 2*A* shows that the decay phase is slower for the hNE current. The rate of inactivation was quantified by fitting the decay phase of the macroscopic current with a single-exponential function. The time constants estimated from these fits are plotted as a function of the test potentials in Figure 2*B*. The time constants were greater for hNE currents than for hSkM1 channels over the entire voltage range from −50 to +30 mV. At 0 mV, for example, hNE currents inactivated with a time constant of 0.77 ± 0.03 msec ($n = 10$), and hSkM1 channels inactivated with a time constant of 0.51 ± 0.05 msec ($n = 10$). This difference was statistically significant ($p < 0.01$).

The voltage dependence of steady-state inactivation (h_∞) was examined by holding the cells at prepulse potentials between −130 and −10 mV for 500 msec before stepping to the test potential (−10 mV) for 20 msec. The h_∞ curves are plotted in Figure 2*C*. The midpoint of the h_∞ curve was significantly ($p < 0.001$) more negative for hNE channels (−78 ± 1 mV; $n = 45$) than for hSkM1 channels (−72 ± 1 mV; $n = 31$).

Because TTX-S currents in DRG neurons recover relatively slowly from inactivation and because hNE transcripts are detected in the majority of DRG neurons (Black et al., 1996), we wanted to compare the time course for recovery from inactivation for hNE and hSkM1 channels. Recovery was examined after 20 msec inactivating pulses at −20 mV (protocol shown in Fig. 3*A*). We used 20 msec inactivating prepulses to allow complete fast inactivation without inducing slow inactivation. Similar results were also obtained with 5 and 100 msec inactivating prepulses (data not shown). Figure 3*A* shows currents from a representative hNE cell and hSkM1 cell illustrating recovery at −80 mV. Although only ~50% of the hNE current has recovered after 100 msec at −80 mV, virtually all of the hSkM1 current has recovered at this time. In general, the time course for recovery from inactivation for both hNE and hSkM1 currents could be fitted well with a single-exponential function. The average recovery time course at −80 mV for hNE and hSkM1 currents is shown in Figure 3*B*. The time constant for recovery of hNE channels (τ = 104 ± 8 msec; $n = 12$) was more than sixfold greater than the corresponding time constant for hSkM1 channels (τ = 16 ± 4 msec; $n = 11$).

We also compared the time course for the development of inactivation of hNE and hSkM1 channels. The protocol for these experiments is shown at the *top* of Figure 3*C*. Cells were stepped

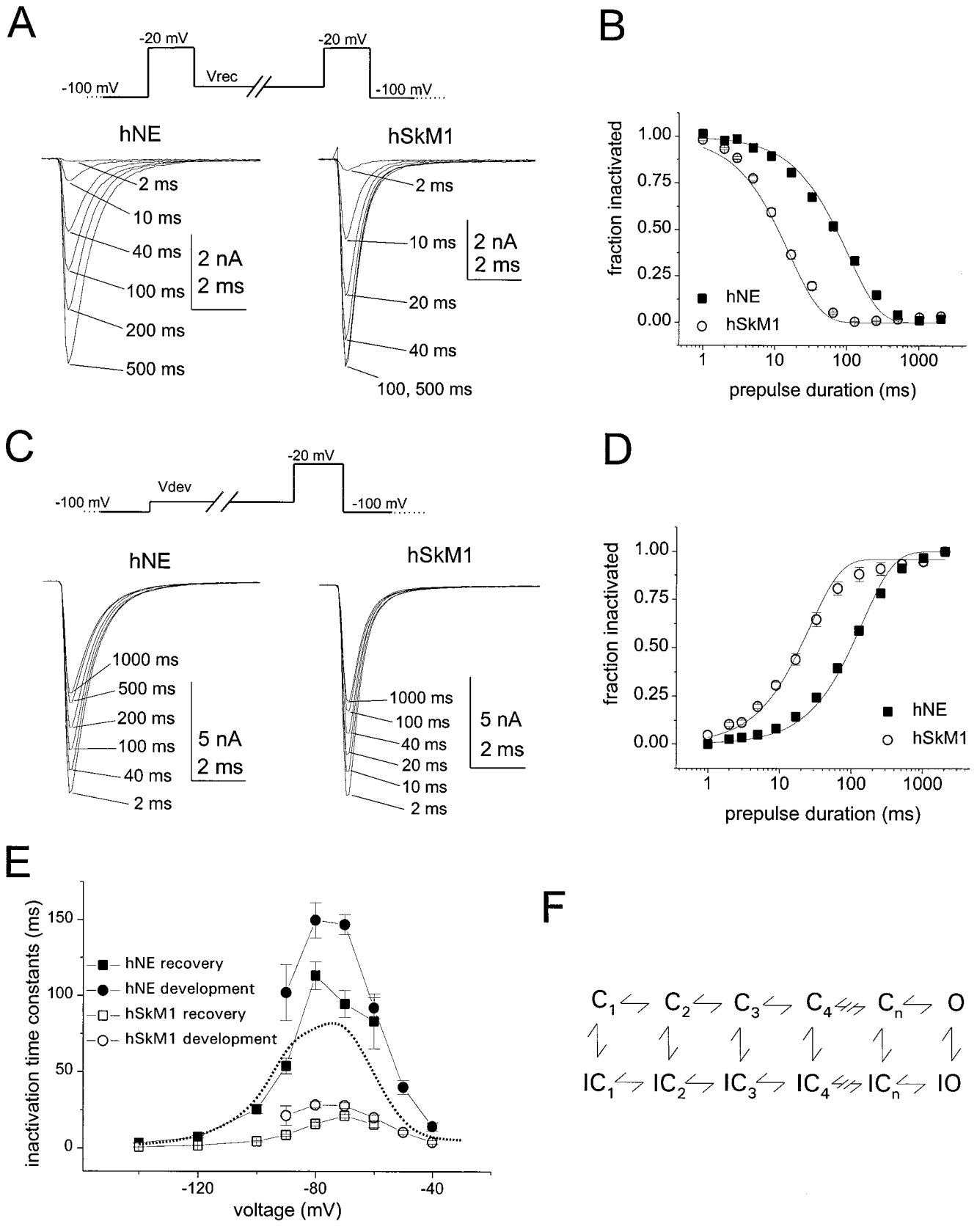

Figure 3. Recovery from inactivation and development of inactivation are slower for hNE channels than for hSkM1 channels. *A*, Family of current *traces* from cells expressing hNE or hSkM1 currents showing the rate of recovery from inactivation at −80 mV. The standard recovery from inactivation voltage protocol is shown *above* the current *traces*. The cells were prepulsed to −20 mV for 20 msec to inactivate all of the current and then brought back to −80 mV for increasing recovery durations before the test pulse to −20 mV. The maximum pulse rate was 0.5 Hz. *B*, Time course for recovery from inactivation of peak currents at −80 mV. Recovery is much slower for hNE (*filled squares*; $n = 12$) than for hSkM1 (*Figure legend continues)*

to the inactivation potential (from a holding potential of −100 mV) for increasing durations and then stepped to the test potential (−20 mV) to measure the fraction of current remaining available. Figure 3*C* shows representative currents illustrating the development of inactivation at −80 mV for hNE and hSkM1 channels. Although less than one-half of the hNE inactivation has occurred after the 100 msec inactivating pulse (at −80 mV), hSkM1 inactivation is nearly complete at this time point. The average time course for development of inactivation at −80 mV from 12 hNE and 11 hSkM1 cells is shown in Figure 3*D*. The data from these cells were fitted well with a single-exponential function, and the time constant was almost fivefold greater for hNE channels (τ = 144 ± 11 msec; n = 12) than for hSkM1 channels (τ = 26 ± 7 msec; n = 11).

The time course for recovery from inactivation was measured at voltages ranging from −140 to −60 mV, and the time course for development of inactivation was measured from −90 to −40 mV for both hNE and hSkM1. At most voltages both the rate of recovery from inactivation and the development of inactivation were much slower for hNE channels (Fig. 3*E*). The time constants for inactivation of hNE currents are similar to those measured for the TTX-S currents in small DRG neurons (Fig. 3*E*, *dotted curve*) (Cummins and Waxman, 1997). By contrast, the predominant time constants measured for cloned rbII channels (Sakar et al., 1995) and the sodium currents in adult hippocampal neurons (Costa, 1996) are similar to those for the hSkM1 channels.

The difference between hNE and hSkM1 inactivation kinetics can be considered in the context of a simple multistate sodium channel gating scheme (Vandenberg and Bezanilla, 1991; Kuo and Bean, 1994) such as that shown in Figure 3*F*. This model has multiple closed states leading to the open state. Channels progress through these closed states during depolarization. In this model, inactivation can occur from any of the closed states as well as from the open state. The rate of macroscopic inactivation at potentials positive to −20 mV is thought primarily to reflect inactivation of channels in the open state. The results shown in Figure 2*B* thus suggest that open-state inactivation is ~50% slower for hNE channels than it is for hSkM1 channels. At potentials less than −60 mV, at which the probability of channel opening is very low, inactivation would occur primarily from the closed states. The time course for the development of inactivation between −90 to −60 mV was much slower for hNE than for hSkM1 channels, and therefore our data indicate that closed-state inactivation is relatively slow for hNE channels.

Recovery from inactivation was also relatively slow for hNE currents compared with hSkM1 currents. However, although the inactivation time constants were dramatically different for hNE and hSkM1 currents, we observed a discrepancy between the rate for development of inactivation and the rate for recovery from inactivation when measured at the same potential (from −90 to −60 mV). This discrepancy was observed for both hNE and hSkM1 currents (Fig. 3*E*). At −80 mV, for example, recovery from inactivation was ~30% faster than was development of inactivation for hNE channels. Similarly, for hSkM1 channels recovery from inactivation at −80 mV was ~40% faster than was development of inactivation at −80 mV. This discrepancy is not completely unexpected, because the development of inactivation and recovery from inactivation protocols examine distinct processes. Although development of inactivation at −80 mV exclusively involves closed-state inactivation, recovery from inactivation, also measured at −80 mV, follows a 20 msec depolarizing step, during which a significant proportion of the channels inactivate from the open state. Thus recovery involves both open-state and closed-state inactivation (Aldrich et al., 1983). Interestingly, although the values for development of inactivation and for recovery from inactivation differed, the values did not differ markedly, and both processes could be reasonably well fit with a single exponential (Fig. 3*B*,*D*). Kuo and Bean (1994) reported that most sodium channels probably must close (i.e., make the IO to IC transition) before recovering from inactivation. Thus the rate of recovery from inactivation also probably reflects primarily the rate of channel transition between the closed-inactivated and closed states.

Functional significance of slow recovery from inactivation

The slow rate for development of closed-state inactivation and recovery from inactivation in hNE channels is intriguing, especially because it is so pronounced at voltages near the typical resting potential for neurons. Slower recovery from inactivation should decrease the maximum firing frequency. Figure 4 shows that during a 50 Hz pulse train the current amplitude remains much higher for cells expressing hSkM1 channels (Fig. 4*A*) than for cells expressing hNE channels (Fig. 4*B*). Although 45 ± 16% of the peak current remains available for the second pulse and 36 ± 17% remains for the 50th pulse for hSkM1 channels (n = 8), only 23 ± 8 and 10 ± 5% remain available for the second and 50th pulses, respectively, for hNE channels (n = 12). The lower availability for hNE channels occurs even though macroscopic inactivation is ~50% slower for hNE channels and more hSkM1 channels presumably inactivate during the 2 msec step depolarizations. Thus, because hNE channels reprime more slowly than do hSkM1 channels, a cell expressing a pure population of hNE channels should not be capable of the high firing frequencies that might be expected in a cell expressing hSKM1 channels. The firing rate is limited by the repriming rate, which probably reflects

←

(open circles; n = 11) currents. The *solid curves* show single-exponential functions fitted to the data, with time constants of 104 msec (hNE) and 16 msec (hSkM1). The data are plotted on a logarithmic time axis to allow comparison of the disparate time courses. *C*, Family of current *traces* from cells expressing hNE and hSkM1 currents showing the rate of development of inactivation at −80 mV. The standard development of inactivation voltage protocol is shown *above* the current *traces*. From a holding potential of −100 mV, the cells were prepulsed to −80 mV for increasing durations and then stepped to −20 mV to determine the fraction of current inactivated during the prepulse. *D*, Time course for development of inactivation for the peak current. Inactivation develops more slowly at −80 mV for hNE channels (*filled squares*; n = 12) than for hSkM1 channels (*open circles*; n = 11). The *solid curves* are single-exponential functions fitted to the data, with time constants of 144 msec (hNE) and 26 msec (hSkM1). *E*, The time constants for recovery from inactivation (*squares*) and development of inactivation (*circles*) plotted as a function of voltage. Time constants were estimated from single-exponential fits to time courses measured with the protocols shown in *A* and *C* for cells expressing hNE channels (*filled symbols*; n = 15) and hSkM1 channels (*open symbols*; n = 11). For comparison the inactivation time constants for the TTX-S current in small DRG neurons are shown (*dotted curve*). *F*, Basic multistate gating scheme for sodium channel activation and fast inactivation. Closed states are indicated by *C*s, inactivated closed states are indicated by *IC*s, the open state is indicated by *O*, and the inactivated open state is indicated by *IO*. At very negative potentials, channels reside in the leftmost closed state, and with depolarization the channels progress toward the open state. Channels can inactivate from any state.

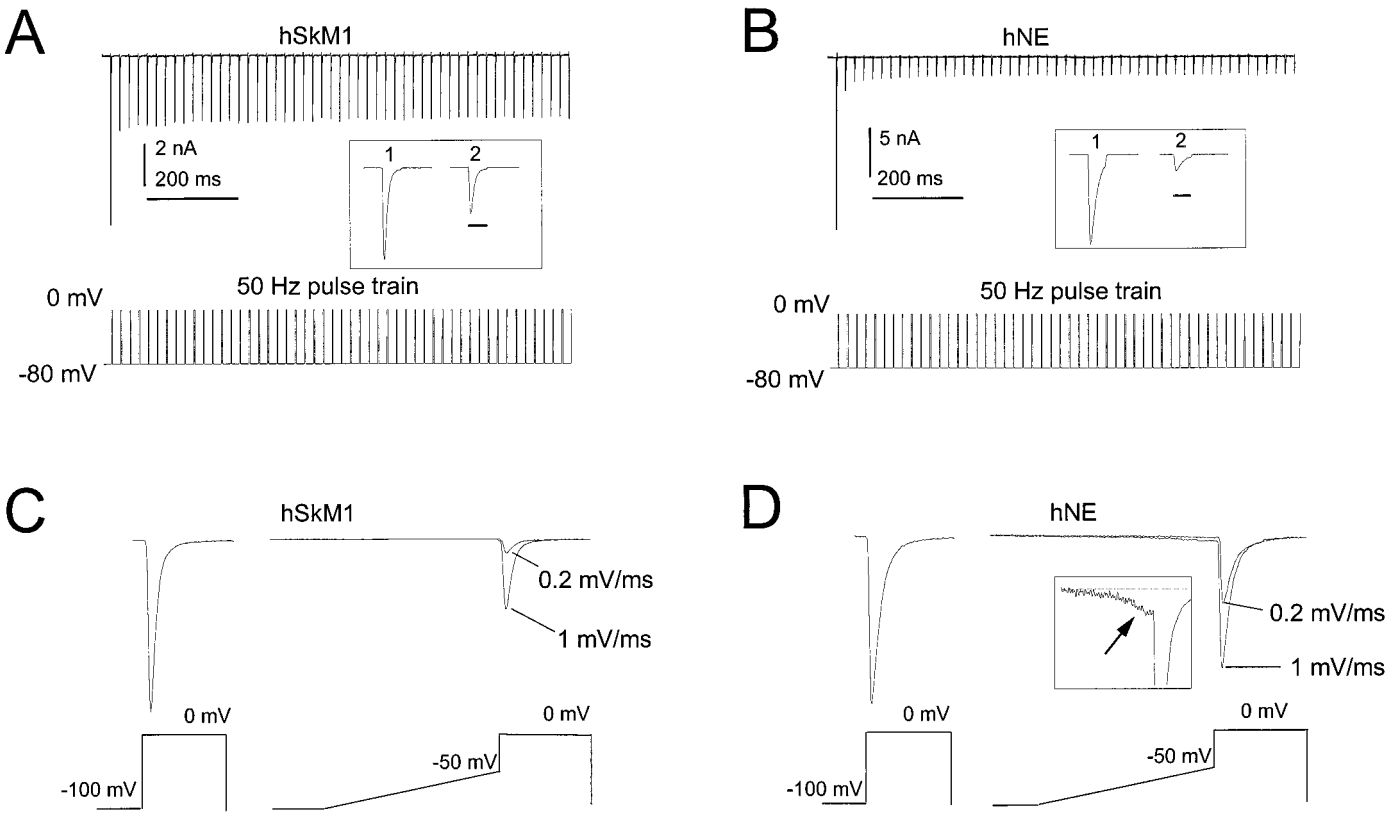

Figure 4. Functional consequences of slow closed-state inactivation. *A*, The sodium currents elicited in a cell expressing hSkM1 channels by a 50 Hz pulse train. The cell, held at −80 mV, was depolarized to 0 mV for 2 msec every 20 msec during the 1 sec pulse train. *Inset*, Currents elicited by the first and second depolarizations on an expanded time scale (calibration bar, 2 msec). The current elicited by the second pulse is approximately one-half the amplitude of the current elicited by the first pulse. *B*, The sodium currents elicited in a cell expressing hNE channels by a 50 Hz pulse train. Details are as described in *A*. The current elicited by the second pulse is much smaller than that elicited by the first pulse. *C*, Comparison of hSkM1 current elicited by a step depolarization to 0 mV from −100 mV (*left trace*) with the hSkM1 current elicited by a step depolarization from −50 mV that was preceded by a slow ramp depolarization from −100 to −50 mV (*right traces*). The voltage protocol is shown *below* the current *traces*. Two different ramp speeds were used: 1 mV/msec (50 msec total duration) and 0.2 mV/msec (250 msec total duration). After the 50 msec ramp, less than one-half of the current remains available for activation, and after the 250 msec ramp, only ~10% of the current is available. *D*, Currents elicited by the voltage protocols detailed in *C* in a cell expressing hNE channels. After the 50 msec ramp, much of the hNE current remains available for activation, and after the 250 msec ramp, more than one-third of the current is still available. *Inset*, The end of the 50 msec ramp depolarization at higher gain. The *arrow* indicates a region where the ramp depolarization elicits an inward current before the step depolarization.

the frequency of transitions between the closed-inactivated and closed states.

Functional significance of slow development of inactivation

The slow rate for the development of closed-state inactivation in hNE channels can also have important consequences. Because closed-state inactivation occurs so slowly, especially at voltages from −90 to −50 mV, short prepulses are not sufficient to reach steady-state conditions for hNE channels. For example, a 50 msec prepulse to −80 mV only allows 30% of the channels to inactivate, compared with 97% for a 500 msec prepulse. As a consequence of this, if "steady-state inactivation" is measured using 50 msec prepulses, the estimated midpoint of the h_∞ curve is significantly more positive for hNE channels (−56 ± 2 mV) than for hSkM1 channels (−70 ± 1 mV).

Based on this observation, we predicted that a large fraction of hNE channels, but not hSkM1 channels, would remain available for activation during slow ramp depolarizations. To test this, cells were slowly depolarized from −100 to −50 mV and then stepped to 0 mV to determine how much current remained available for activation. For hSkM1 channels (Fig. 4*C*), 37 ± 19% (n = 9) of the current remained available after a 50 msec (1 mV/msec) ramp, and only 10 ± 12% remained after a 250 msec (0.2 mV/msec) ramp. In contrast, significantly more current remained available for hNE channels (Fig. 4*D*), with 76 ± 10% (n = 14) of the current available after the 50 msec ramp and 36 ± 13% still available after the 250 msec ramp. Thus, although neurons expressing faster repriming channels may be capable of firing at higher frequencies, neurons expressing hNE channels should be able to generate action potentials in response to slowly rising inputs that do not elicit a regenerative response in neurons expressing channels with fast closed-state inactivation.

Slow ramp currents can be evoked in hNE channels

As can be seen in the *inset* in Figure 4*D*, during some of the ramp and step experiments on cells expressing hNE channels, a small inward current was observed during the slow ramp. This was further examined using extended ramp depolarizations that ranged from −100 to 40 mV. These slow ramps (0.23 mV/msec) elicited little or no current in cells expressing hSkM1 channels (Fig. 5*A*), but prominent currents were evoked in cells expressing hNE channels (Fig. 5*B*). The hNE ramp currents were 1.7 ± 0.2% (n = 11) of the peak current amplitude (obtained in re-

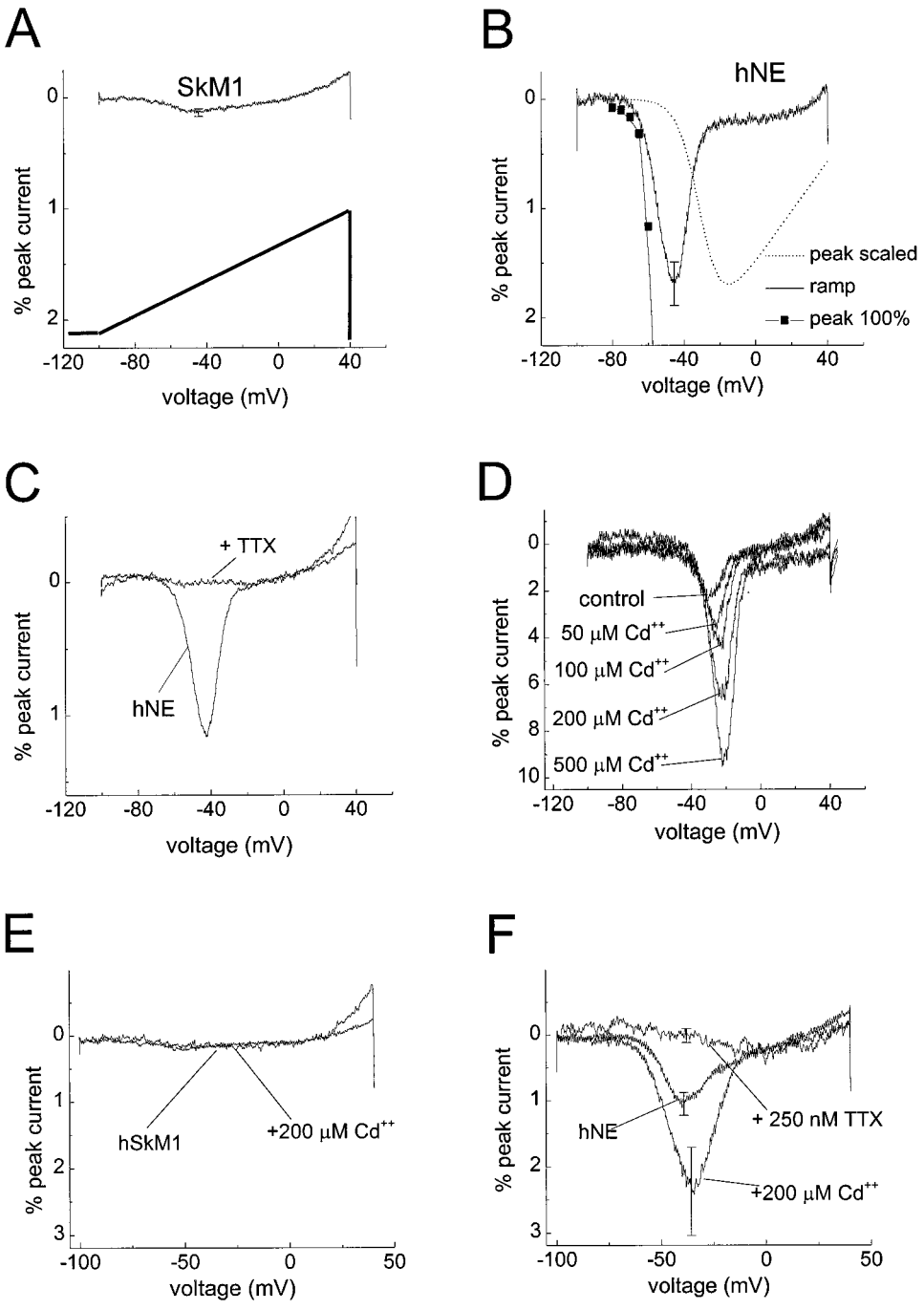

Figure 5. Characterization of ramp currents. Ramp currents were examined using 600 msec voltage ramps from −100 to +40 mV (~0.23 mV/msec). *A*, The average ramp current recorded in cells expressing hSkM1 channels ($n = 12$). The *thick solid line* at the *bottom* illustrates the ramp voltage protocol. The ramp current is plotted as a percentage of the peak sodium current elicited with step depolarizations from −100 mV. The error bar indicates the SE at −45 mV. *B*, The average ramp current recorded in cells expressing hNE channels ($n = 11$). The ramp current is plotted as a percentage of the peak sodium current elicited with step depolarizations from −100 mV. The error bar indicates the SE at −45 mV. The *dotted curve* shows the averaged current–voltage (*I–V*) relationship for the peak current elicited with step depolarizations in these cells scaled to the amplitude of the ramp current. The *filled squares* show the peak *I–V* data at full scale. Only the foot of the curve can be seen at this scale. The step depolarizations to −60 mV elicited ~1.2% of the current elicited by the step depolarizations to −15 mV. *C*, Current *traces* elicited in an hNE cell by 600 msec ramps. The current (plotted as a percentage of peak current) is shown before and after the addition of 250 nM TTX to the extracellular solution. TTX blocks the ramp current. *D*, Current *traces* elicited in an hNE cell by 600 msec ramps shown before and after the addition of increasing concentrations of cadmium (50–500 μM Cd^{2+}) to the extracellular solution. Cadmium increases the amplitude of the ramp current in hNE cells. *E*, The average currents elicited by 600 msec ramps in cells expressing hSkM1 channels shown before and after addition of 200 μM cadmium to the extracellular solution ($n = 4$). Cadmium does not induce hSkM1 ramp currents. *F*, The average currents elicited by 600 msec ramps in cells expressing hNE channels shown before and after addition of 200 μM cadmium to the extracellular solution ($n = 5$). Cadmium increased the amplitude of the ramp current by ~150%, and all of the ramp current in cadmium was blocked by 250 nM TTX. Error bars indicate SE at −40 mV.

sponse to stimulation with step depolarizations to −10 mV) and, when compared with the scaled peak current–voltage relationship, reach maximal amplitude at potentials ~20 mV more negative than the peak currents (Fig. 5*B*). This type of ramp current, often referred to as "subthreshold" or persistent current, has been recorded in several different types of neurons (Stafstrom et al., 1985; Brown et al., 1994; Cepeda et al., 1995; Chao and Alzheimer, 1995; Fleidervish and Gutnick, 1996; Pennartz et al., 1997; Raman and Bean, 1997; Feigenspan et al., 1998; Parri and Crunelli, 1998). It has been proposed that, because neuronal ramp currents occur near resting potentials and are often larger than other voltage-gated currents at these potentials, ramp currents may significantly influence excitability (Crill, 1996). Indeed, it has been shown that persistent sodium currents in the dendrites of neocortical neurons can help boost transmission of synaptic depolarizations (Schwindt and Crill, 1995).

The narrow voltage range in which hNE ramp currents are recorded is very similar to that for ramp currents recorded in neurons. The mechanism underlying the distinct voltage dependence of neuronal ramp currents has not been completely understood. Because ramp currents seem to be activated at more negative potentials than the currents elicited with step depolarizations, it has been suggested that distinct channel populations might underlie ramp currents and transient currents in neurons. In the HEK293 cells the ramp and transient currents are probably generated by the same channel isoform. Indeed, the apparent

difference in voltage dependence, at least for hNE channels, is an artifact that results from the scaling of the peak current–voltage curve to the size of the ramp current. The ramp current at −55 mV and the peak current elicited with a step depolarization to −55 mV are both ~1% of the maximum peak current (measured with step depolarizations). When the peak current data are plotted at full scale (Fig. 5*B*, *solid squares*), it is clear that the foot of the peak current–voltage relationship closely matches the voltage dependence of the onset of the ramp current.

Our data indicate that the ramp currents are observed at −60 mV because hNE channels, with slow closed-state inactivation kinetics, do not all inactivate during slow ramps and therefore some remain available for activation. Conversely, although a step depolarization to −55 mV activates 1.9 ± 0.6% (n = 10) of the peak current for hSkM1 channels, almost no hSkM1 current is observed during slow ramp depolarizations because the hSkM1 channels undergo rapid closed-state inactivation and are inactivated during slow depolarizations before reaching the open state. The decay of the ramp currents at more depolarized voltages probably reflects channels undergoing open-state inactivation, which is still relatively fast in hNE channels. Therefore, our results suggest that the distinct voltage dependence of ramp currents does not necessarily arise from unique activation properties of the underlying sodium channels but rather from their distinctive inactivation kinetics.

hNE ramp currents are differentially sensitive to TTX and cadmium

To confirm that the ramp currents recorded in hNE cells were sodium currents, we tested the pharmacology of the ramp currents with nanomolar concentrations of TTX, which blocks hNE channels, and micromolar concentrations of cadmium, which does not block hNE channels (Klugbauer et al., 1995) but does block voltage-gated calcium channels. Figure 5*C* shows that the hNE ramp currents were blocked by 250 nM TTX. The effect of cadmium on hNE ramp currents is illustrated in Figure 5*D*. Surprisingly, cadmium increased the size of the ramp currents, at concentrations that are equal to or lower than those routinely used in the isolation of sodium currents (Brown et al., 1994; Cepeda et al., 1995; Fleidervish and Gutnick, 1996; Pennartz et al., 1997; Raman and Bean, 1997; Parri and Crunelli, 1998). In five cells expressing hNE channels, 200 μM cadmium increased the size of the ramp currents by 160 ± 17%, and the total ramp current was also blocked by TTX (Fig. 5*F*). By contrast, cadmium did not induce ramp currents in cells expressing hSkM1 channels (Fig. 5*E*).

To understand how cadmium increased ramp currents, we examined the effect of cadmium on the other properties of hNE and hSkM1 currents. Cadmium (200 μM) had little effect on hNE peak current amplitude, which was decreased by 5 ± 5% (n = 8). Cadmium also did not significantly alter noninactivating hNE currents (0.35 ± 0.16% of peak, control; 0.29 ± 0.14% in 200 μM Cd^{2+}; n = 6), measured at 100 msec during a step depolarization to 0 mV. The midpoints of activation (−27 ± 2 mV, control; −27 ± 3 mV, cadmium; n = 8) and steady-state inactivation (−77 ± 3 mV, control; −74 ± 4 mV, cadmium; n = 8) for hNE currents were not significantly altered by 200 μM cadmium. Similarly, cadmium did not alter these properties in hSkM1 channels (data not shown).

However, as can be seen in Figure 6*A*, 200 μM cadmium did prolong the time course for the development of closed-state inactivation in hNE channels. In seven cells, 200 μM cadmium

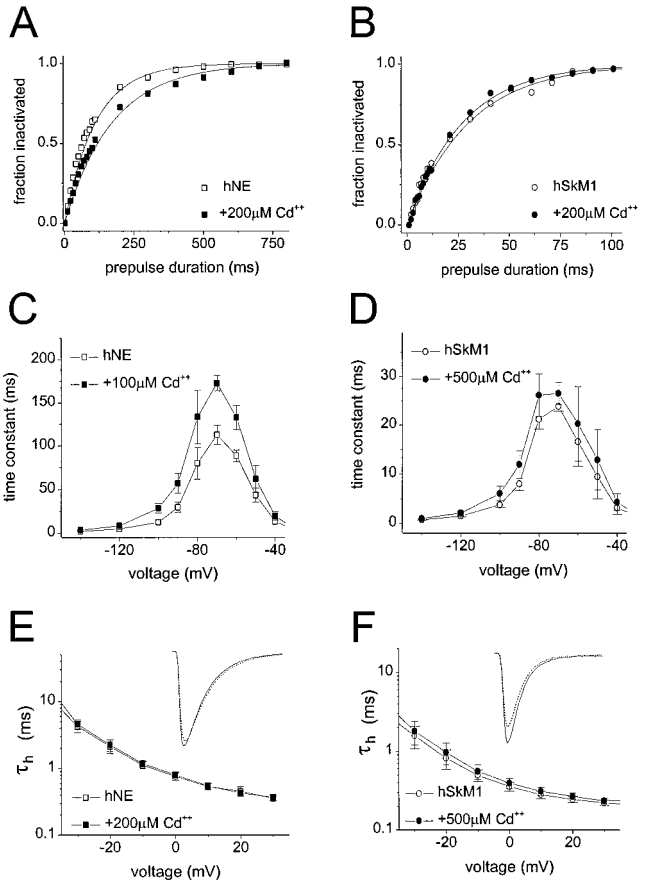

Figure 6. Cadmium modulates closed-state inactivation in hNE but not in hSkM1 channels. *A*, Cadmium slows the development of sodium current inactivation in a cell expressing hNE channels. The time course for development of inactivation at −80 mV is shown before (*open squares*) and after (*filled squares*) addition of 200 μM Cd^{2+} to the extracellular solution. The *solid curves* are single-exponential functions fit to the hNE data before (τ = 96 msec) and after (τ = 155 msec) cadmium. *B*, Cadmium does not slow the development of sodium current inactivation in a cell expressing hSkM1 channels. The time course for development of inactivation at −80 mV is shown before (*open circles*; τ = 29 msec) and after (*filled circles*; τ = 26 msec) addition of 200 μM Cd^{2+} to the extracellular solution. Please note the difference in the *x*-axis scales between *A* and *B*. *C*, The inactivation time constants between −140 and −40 mV for Na^+ currents in cells expressing hNE cells (n = 5) are shown before (*open squares*) and after (*filled squares*) addition of 100 μM Cd^{2+} to the extracellular solution. At voltages at which both development of inactivation and recovery from inactivation were measured (i.e., between −60 and −90 mV), the inactivation time constant was estimated by averaging the development of inactivation and recovery from inactivation time constants. *D*, The inactivation time constants between −140 and −40 mV for Na^+ currents in cells expressing hSkM1 cells (n = 4) are shown before (*open circles*) and after (*filled circles*) addition of 500 μM Cd^{2+} to the extracellular solution. Note the difference in the *y*-axis scales between *C* and *D*. *E*, The inactivation time constants for open-state inactivation (τ_h) measured from single-exponential fits to the decay of currents elicited by step depolarizations to voltages between −30 and +30 mV for Na^+ currents in cells expressing hNE channels (n = 6) are shown before (*open squares*) and after (*filled squares*) addition of 200 μM Cd^{2+} to the extracellular solution. *Inset*, Current *traces* are from a representative hNE cell before (*solid trace*) and after (*dashed trace*) cadmium. *F*, Plots of τ_h measured at voltages between −30 and +30 mV for Na^+ currents in cells expressing hSkM1 channels (n = 4) are shown before (*open circles*) and after (*filled circles*) addition of 500 μM Cd^{2+} to the extracellular solution. *Inset*, Current *traces* are from a representative hSkM1 cell before (*solid trace*) and after (*dashed trace*) cadmium.

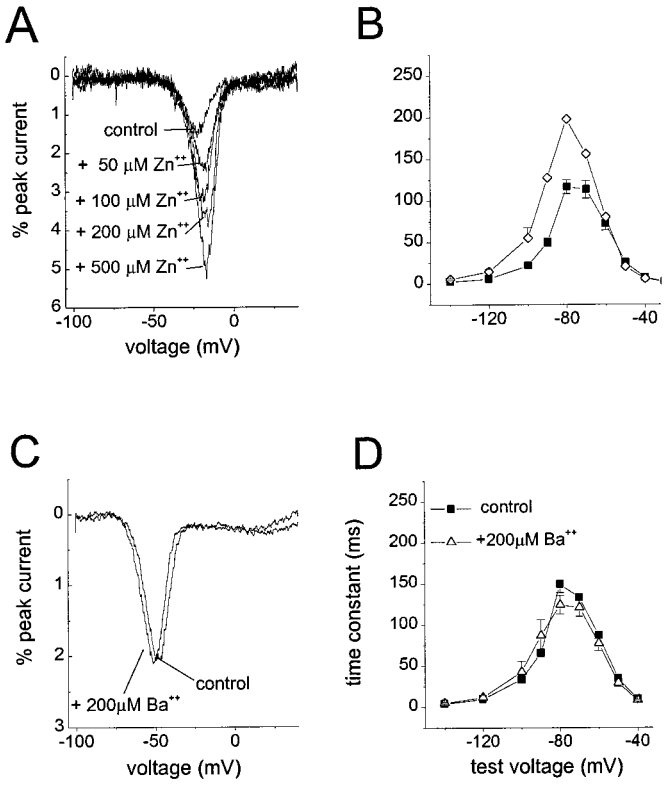

Figure 7. Zinc, but not barium, also modulates hNE closed-state inactivation and increases hNE ramp currents. *A*, Current *traces* elicited in an hNE cell by 600 msec ramps are shown before and after the addition of increasing concentrations of zinc (50–500 μM) to the extracellular solution. Zinc increases the amplitude of the ramp current in hNE cells. *B*, The inactivation time constants between −140 and −40 mV for Na^+ currents in cells expressing hNE cells ($n = 4$) are shown before (*filled squares*) and after (*open diamonds*) addition of 100 μM Zn^{2+} to the extracellular solution. *C*, Currents elicited by 600 msec ramps in an hNE cell are shown before and after addition of 200 μM barium to the extracellular solution. Barium does not increase hNE ramp currents ($n = 4$). *D*, The inactivation time constants between −140 and −40 mV for Na^+ currents in cells expressing hNE ($n = 6$) are shown before (*filled squares*) and after (*open triangles*) addition of 200 μM Ba^{2+} to the extracellular solution.

increased the time constant for the development of inactivation at −80 mV by 61 ± 17% and increased the time constant for recovery from inactivation at −80 mV by 46 ± 12%. These differences were significant (paired *t* test, $p < 0.005$). In contrast, 200 μM cadmium did not affect the time course for development of closed-state inactivation in hSkM1 channels (Fig. 6*B*). Even at higher concentrations (500 μM), cadmium had little effect on hSkM1 channels, increasing the time constant for the development of inactivation at −80 mV by only 7 ± 6% and the time constant for recovery from inactivation at −80 mV by only 6 ± 4%. Although Figure 6*C* shows that even 100 μM cadmium greatly increased the inactivation time constants for hNE channels at voltages ranging from −100 to −50 mV, Figure 6*D* demonstrates that 500 μM cadmium had little effect on the inactivation time constants of hSkM1 channels in this voltage range. This demonstrates that the lack of effect of cadmium on hSkM1 channels was not simply a slight difference in sensitivity to cadmium. Interestingly, cadmium had no effect on the rate of decay of macroscopic currents (evoked by step depolarizations ranging from −30 to +30 mV) for either hNE channels (200 μM; Fig. 6*E*) or hSkM1 channels (500 μM; Fig. 6*F*). This indicates that cadmium primarily slows closed-state inactivation but not open-state inactivation of hNE channels. This also provides additional evidence to support the hypothesis that slow closed-state inactivation of hNE channels underlies the generation of ramp currents.

Some, but not all, divalent cations modulate hNE channels, and this is illustrated in Figure 7. Zinc, like cadmium, increased hNE ramp currents (Fig. 7*A*) and also increased the inactivation time constants for closed-state inactivation at negative potentials (Fig. 7*B*). Cobalt (200 μM) had a slightly less pronounced effect (data not shown) then did cadmium and zinc, whereas barium (200 μM) had virtually no effect on hNE ramp currents (Fig. 7*C*) and on hNE inactivation time constants (Fig. 7*D*). These data also support the link between slow closed-state inactivation and the generation of ramp currents.

Ramp currents and slow closed-state inactivation in DRG neurons

Because hNE is expressed in a majority of small DRG neurons (Black et al., 1996) and the TTX-S sodium current in small DRG neurons has slow closed-state inactivation kinetics (Elliott and Elliott, 1993; Cummins and Waxman, 1997), we tested whether cadmium also modulated DRG TTX-S currents. We used 100 μM cadmium for these experiments because this concentration was used in studies by others (Parri and Crunelli, 1998) and in our previous studies on repriming kinetics in small DRG neurons (Cummins and Waxman, 1997). Figure 8, *A* and *B*, shows that cadmium slowed the development of inactivation for the TTX-S current in small DRG neurons. Cadmium had a dramatic effect on the time constants of inactivation for DRG TTX-S channels at potentials ranging from −100 to −60 mV (Fig. 8*C*). Small DRG neurons also displayed ramp currents that were increased by cadmium and blocked by TTX (Fig. 8*D*). In four cells, 100 μM cadmium increased the amplitude of the ramp current by 45 ± 6%. The ramp current recorded in 100 μM cadmium was 1.9 ± 0.3% ($n = 6$) of the peak TTX-S fast sodium current in small DRG neurons, compared with 1.7 ± 0.2% ($n = 9$) for hNE ramp currents in 100 μM cadmium.

There is an apparent difference between the voltage dependence of DRG TTX-S peak current elicited with step depolarizations and that of the ramp current (Fig. 9*A*). However, as was shown for hNE currents in Figure 5*B*, this apparent difference is an artifact that results from the scaling of the peak current curve to the size of the ramp currents. The *solid squares* in Figure 9*A* show that when the peak current data are plotted at full scale, the threshold for activation of DRG TTX-S currents elicited with step depolarizations is similar to that for the DRG TTX-S ramp current. Although multiple sodium channels probably contribute to the excitability of DRG neurons, these data support the hypothesis that a single sodium channel isoform can underlie both a peak transient TTX-S current and a TTX-S ramp current and argue against the need to invoke multiple channel populations to account for these currents. Figure 9*B* shows that the voltage dependences of the TTX-S ramp and peak currents in small DRG neurons were nearly identical to those of the hNE currents recorded in HEK293 cells under the same conditions. This is consistent with the data indicating that the hNE transcript is expressed in a majority of small neurons. Because hNE channels and DRG TTX-S currents both exhibit slow closed-state inactivation and because cadmium can modulate closed-state inactivation and increase ramp currents in both DRG neurons and in

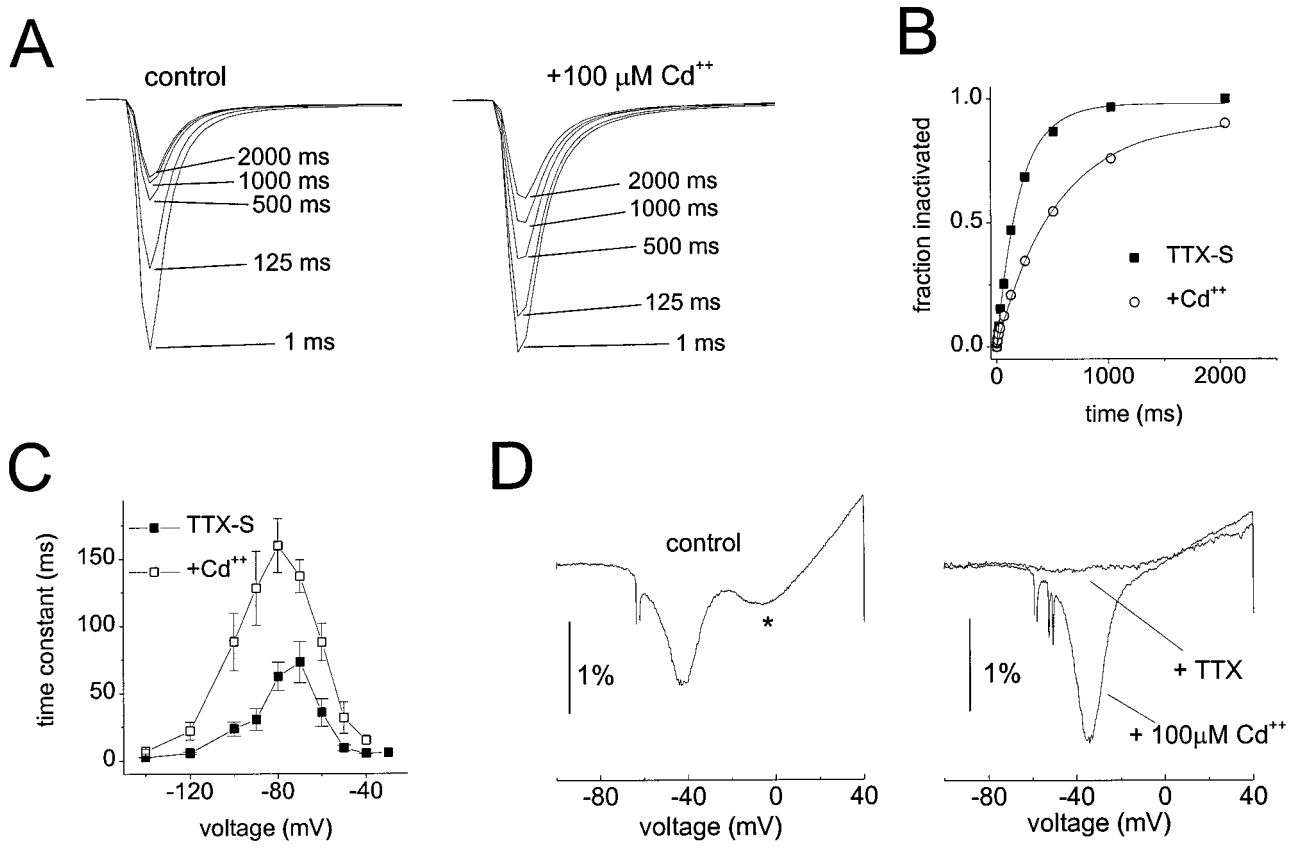

Figure 8. Cadmium modulates closed-state inactivation and ramp currents in DRG neurons. *A*, Families of current *traces* from a small DRG neuron (21 μm in diameter) before (*left*) and after (*right*) application of 100 μM Cd^{2+} to the extracellular solution show that the rate of development of inactivation at −80 mV is slowed by Cd^{2+}. The TTX-S peak current amplitude was 98% of the total peak current amplitude in this cell. *B*, Time course for development of inactivation of the peak current before (*filled squares*) and after (*open circles*) application of 100 μM Cd^{2+}. Data are from the currents shown in *A*. *C*, The inactivation time constants between −140 and −40 mV for TTX-S Na^+ currents in small (18–25 μm) DRG neurons from adult rats ($n = 6$) are shown before (*filled squares*) and after (*open squares*) addition of 100 μM Cd^{2+} to the extracellular solution. Data were obtained with the same two-pulse protocol described in Figure 3*C*. The TTX-S peak current amplitude was 75 ± 4% ($n = 6$) of the total peak current amplitude for these cells. *D*, Ramp current recorded in a small DRG neuron before (*left*) and after (*right*) addition of 100 μM Cd^{2+} to the extracellular solution. Cd^{2+} increases the ramp current component that peaks near −40 mV. This component is blocked by 250 nM TTX (*right*). A second component (*left*; marked by the *asterisk*) is apparently blocked by Cd^{2+} and may therefore be a calcium current. The ramp, which extended from −100 to +40 mV, was 600 msec long. The scale bar indicates the percentage of the peak current amplitude measured with a step depolarization to −10 mV.

HEK293 cells expressing hNE channels, a similar mechanism probably underlies the ramp currents in both preparations.

DISCUSSION

We have compared the functional properties of hNE and hSkM1 sodium channels expressed in HEK293 cells. Our data show that although the voltage dependences of activation and steady-state inactivation are similar for hNE and hSkM1 channels, hNE channels display slower open-state inactivation, slower closed-state inactivation, and slower recovery from inactivation than do hSkM1 channels. We also observed relatively large TTX-sensitive currents during ramp depolarizations in cells expressing hNE, but not hSkM1, channels.

Mechanism underlying hNE ramp currents

Our results indicate that ramp currents arise in hNE channels because the hNE channels have slow closed-state inactivation. Closed-state inactivation and recovery from inactivation were up to 500% slower for hNE channels than for hSkM1 channels. Because closed-state inactivation develops much more slowly for hNE than for hSkM1 channels, hNE channels are less likely to inactivate during slow subthreshold depolarizations and are more likely to be available to open when the voltage reaches threshold. This mechanism is consistent with the voltage dependence of the ramp currents. As Figure 5*B* shows, the ramp currents and the currents elicited with step depolarizations have similar thresholds.

Although the generation of ramp currents by slow closed-state inactivation can be described by a model such as that shown in Figure 3*F*, it should be noted that this model is probably incomplete. For example, hNE channels also display slow inactivation (data not shown), a kinetically and functionally distinct process from fast inactivation. TTX-S currents in rabbit Schwann cells (from which NaS, the rabbit ortholog of hNE, was cloned) exhibit at least three kinetically distinct types of inactivation (Howe and Ritchie, 1992). Therefore it is likely that hNE, PN1, and NaS exhibit complex inactivation characteristics in addition to the distinctive closed-state inactivation properties described here.

Our data do not eliminate the possibility that persistent currents can also arise from other sodium channel isoforms or from different mechanisms. Several mechanisms have been proposed to underlie persistent sodium currents in neurons: (1) window currents, (2) modal gating, and (3) distinct channel isoforms (Crill,

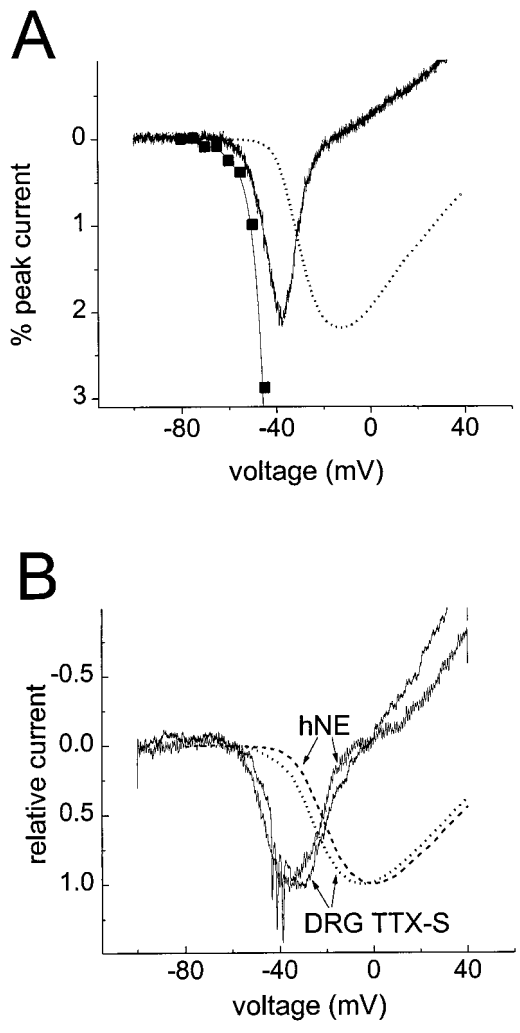

Figure 9. The thresholds for activation of ramp currents and peak transient currents are similar. *A*, The ramp current recorded in a small DRG neuron expressing predominantly TTX-S sodium current. The ramp current is plotted as a percentage of the peak sodium current elicited with step depolarizations from −100 mV. The *dotted curve* shows the current–voltage (*I–V*) relationship for the peak current elicited with step depolarizations in this cell scaled to the amplitude of the ramp current. The *filled squares* show the peak *I–V* data at full scale; only the foot of the curve can be seen at this scale. The ramp, which extended from −100 to +40 mV, was 600 msec long. The access resistance for this cell was 2 MΩ, and 80% series resistance compensation was used. *B*, Comparison of ramp currents in small DRG neurons that expressed predominantly TTX-S currents ($n = 5$) and in HEK293 cells expressing hNE channels ($n = 9$). The currents, elicited with 600 msec ramps that extended from −100 to +40 mV, were normalized for comparison of voltage dependence. The peak current–voltage curves (*dotted* and *dashed lines*) for the cells from which the ramp currents were recorded are also shown. Note that both the DRG TTX-S and the hNE ramp currents reach maximum amplitude ~20 mV more negative than did the peak currents.

1996). Indeed, in DRG neurons persistent window currents can arise from TTX-resistant channels (Cummins and Waxman, 1997), and Alzheimer et al. (1993) demonstrated with single-channel recordings that CNS sodium channels can generate persistent currents by switching between different gating modes. Although these previously described mechanisms may provide an explanation for some of the persistent sodium current in neurons, our results show that persistent threshold currents can be generated by a fourth mechanism, slow closed-state inactivation. Indeed, this mechanism can account for the threshold ramp currents that have been observed in many neuronal preparations without invoking distinct channel populations.

It is not clear which channel structures are responsible for the slow closed-state inactivation in hNE. Several studies (Ji et al., 1996; Dib-Hajj et al., 1997; Chen et al., 1998) have implicated the S3–S4 linker of domain 4 as being important in repriming kinetics. Interestingly, there is a threonine (T1590) in the domain 4 S3–S4 linker of hNE (and NaS) at a position where most of the other sodium channel isoforms, including hSkM1 and rBII, have a lysine. However, rat PN1 (Sangameswaran et al., 1997; Toledo-Aral et al., 1997) also has a lysine at this position, suggesting that other parts of the channel might determine the slow closed-state inactivation of hNE channels. The only consistent difference between the hNE, NaS, and PN1 clones and hSkM1 and rBII in a region previously identified as playing a prominent role in inactivation is in the S4–S5 linker of domain 3 (Yang et al., 1994). Although hNE, NaS, and PN1 have an isoleucine at position 1304, hSkM1 and rBII have a leucine. This is a conservative substitution, but Smith and Goldin (1997) recently published compelling evidence indicating that the nearby alanine at position 1302 (hNE numbering) interacts directly with the putative inactivation particle for rBII.

Divalent modulation of closed-state inactivation and ramp currents

The hypothesis that slow closed-state inactivation underlies ramp currents is supported by our data demonstrating that hNE currents are modulated by cadmium and zinc. These data show that cadmium and zinc increase the time constants for closed-state inactivation of the hNE sodium channels and increase the amplitude hNE ramp currents but have little effect on other channel properties. Although cadmium had no significant effect on hSkM1 currents, cadmium and zinc may modulate the development of inactivation and recovery from inactivation for other neuronal sodium channel isoforms. Indeed we have seen similar effects on rbII channels expressed in Chinese hamster ovary cells (T. R. Cummins, J. R. Howe, and S. G. Waxman, unpublished observations). Cadmium is commonly used in studies of sodium currents because at 0.1–0.5 mM concentrations it blocks calcium channels but not neuronal sodium currents (Klugbauer et al., 1995; Fozzard and Hanck, 1996). Virtually all of the previous studies on TTX-sensitive ramp currents in neurons used cadmium in the extracellular solution. Our results show that cadmium should be used cautiously when studying sodium currents.

In addition to the mechanistic implications of the cadmium and zinc modulation, these effects might also have physiological relevance. Cadmium has been shown to induce pathological changes in the CNS (Wong and Klaassen, 1982) and in sensory ganglia and peripheral nerve (Gabbiani et al., 1967; Sato et al., 1978). Although there is evidence suggesting that the Cd^{2+}-induced injury of white matter may result from disruption of mitochondrial function (Fern et al., 1996), our data raise the possibility that the enhancement of threshold sodium currents [which are known to contribute to white matter injury (Stys et al., 1993)] by cadmium might also contribute to the toxicity of cadmium. The modulation of sodium currents by zinc is intriguing for several reasons. Zinc can be coreleased with neurotransmitters at synapses (Frederickson and Moncrieff, 1994), raising the possibility that zinc could act as a modulator of dendritic sodium currents. It has also been reported that zinc can affect susceptibility to epileptic seizures (Fukahori and Itoh, 1990) and can modulate no-

ciceptive impulse trafficking (Izumi et al., 1995), which involves small DRG neurons.

Functional consequences of slow closed-state inactivation and ramp currents

We have shown that hNE currents are similar to the TTX-S current in small DRG neurons, particularly with respect to the slow rate of closed-state inactivation and the properties of the ramp currents. The distinct properties of hNE sodium channels are expected to have important consequences for cellular excitability. For example, a cell expressing only hNE sodium channels would not be expected to be able to sustain high repetitive firing rates that might be sustained by a cell expressing hSkM1 channels. Conversely, the hNE cell would be expected to respond to slow depolarizing inputs that the hSkM1 cell could not respond too. Gilly and Armstrong (1984) proposed that threshold sodium currents could play an important role in impulse initiation and pacemaking. Because DRG TTX-S and hNE ramp currents can be evoked at potentials close to the resting potential of DRG neurons, they might contribute to the TTX-sensitive oscillations in resting membrane potential that have been observed in these cells (Study and Kral, 1996; Kapoor et al., 1997). Baker and Bostock (1997) proposed that persistent threshold sodium currents in DRG neurons might alternatively play an important role in amplifying depolarizing inputs. This is an intriguing possibility, especially because hNE transcripts (in contrast to other sodium channel transcripts) can be detected in virtually all DRG neurons (Black et al., 1996) and PN1 (the rat ortholog of hNE) immunoreactivity is reportedly highest in the growth cones of cultured rat DRG neurons (Toledo-Aral et al., 1997), suggesting that hNE/PN1/NaS is targeted to nerve terminals. This would situate it ideally for amplifying excitatory inputs.

Belcher et al. (1995) and Sangameswaran et al. (1997) reported that hNE/PN1/NaS mRNA can also be detected in CNS tissues, raising the possibility that this isoform could underlie threshold currents in other neuronal populations. Slow ramp depolarizations have been shown to induce TTX-sensitive ramp currents in many CNS neurons, including neocortical neurons (Stafstrom et al., 1985; Brown et al., 1994; Fleidervish and Gutnick, 1996), thalamocortical neurons (Parri and Crunelli, 1998), suprachiasmatic neurons (Pennartz et al., 1997), neostriatal neurons (Cepeda et al., 1995; Chao and Alzheimer, 1995), cerebellar Purkinje cells (Raman and Bean, 1997), and retinal amacrine cells (Feigenspan et al., 1998). Although CNS sodium currents seem to have predominantly fast repriming kinetics, slowly repriming sodium currents have been recorded in CNS neurons (Martina and Jonas, 1997). Sodium currents with slow repriming may be especially important in dendrites of CNS neurons (Colbert et al., 1997; Jung et al., 1997). However, some studies indicate that hNE or PN1 expression is restricted to the peripheral nervous system (Felts et al., 1997; Toledo-Aral et al., 1997), and it is likely that other isoforms can contribute to the ramp currents in CNS neurons. Indeed, recent evidence has indicated that Na6 underlies a large proportion of the ramp current in cerebellar Purkinje cells (Raman et al., 1997). It is not known whether Na6 channels, or any of the other channels isolated from brain, also have slow closed-state inactivation.

Conclusion

We have studied Na^+ currents produced by the hNE or PN1 sodium channel and have shown that hNE channels have slow closed-state inactivation. Our data show that this provides a previously unrecognized mechanism for the generation of threshold ramp currents and that these ramp currents are subject to modulation. Our results also demonstrate the presence of ramp currents, with voltage dependence and pharmacological characteristics very similar to those of hNE currents, in DRG neurons, which express PN1. Because threshold ramp currents might play a role in the amplification of synaptic inputs, impulse initiation or the generation of pacemaker potentials in neurons, expression of PN1 and this novel modulation could influence the excitability of DRG neurons. Based on these observations, we propose that the kinetics of sodium channel closed-state inactivation may be an important factor in determining the integrative and firing properties of neurons.

REFERENCES

Akopian AN, Sivilotti L, Wood JN (1996) A tetrodotoxin-resistant voltage-gated sodium channel expressed by sensory neurons. Nature 379:257–262.

Aldrich RW, Corey DP, Stevens CF (1983) A reinterpretation of mammalian sodium channel gating based on single channel recording. Nature 306:436–441.

Alzheimer C, Schwindt PC, Crill WE (1993) Modal gating of persistent Na^+ current in pyramidal neurons from rat and cat sensorimotor cortex. J Neurosci 13:660–673.

Baker MD, Bostock H (1997) Low-threshold persistent sodium current in rat large dorsal root ganglion neurons in culture. J Neurophysiol 77:1503–1513.

Belcher SM, Zerillo CA, Levenson R, Ritchie JM, Howe JR (1995) Cloning of a sodium channel α subunit from rabbit Schwann cells. Proc Natl Acad Sci USA 92:11034–11038.

Black JA, Waxman SG (1996) Sodium channel expression: a dynamic process in neurons and non-neuronal cells. Dev Neurosci 18:139–152.

Black JA, Dib-Hajj S, McNabola K, Jeste S, Rizzo MA, Kocsis JD, Waxman SG (1996) Spinal sensory neurons express multiple sodium channel a-subunit mRNAs. Mol Brain Res 43:117–132.

Brown AM, Schwindt PC, Crill WE (1994) Different voltage dependence of transient and persistent Na^+ currents is compatible with modal-gating hypothesis for sodium channels. J Neurophysiol 71:2562–2565.

Caffrey JM, Eng DL, Black JA, Waxman SG, Kocsis JD (1992) Three types of sodium channels in adult rat dorsal root ganglion neurons. Brain Res 592:283–297.

Cepeda C, Chandler SH, Shumate LW, Levine MS (1995) Persistent Na^+ conductance in medium-sized neostriatal neurons: characterization using infrared videomicroscopy and whole cell patch-clamp recordings. J Neurophysiol 74:1343–1348.

Chao TI, Alzheimer C (1995) Do neurons from rat neostriatum express both TTX-sensitive and a TTX-insensitive slow Na^+ current? J Neurophysiol 74:934–941.

Chen QY, Kirsch GE, Zhang DM, Brugada R, Brugada J, Brugada P, Potenza D, Moya A, Borggrefe M, Breithardt G, Ortizlopez R, Wang Z, Antzelevitch C, Obrien RE, Schulzebahr E, Keating MT, Towbin JA, Wang Q (1998) Genetic basis and molecular mechanism for idiopathic-ventricular fibrillation. Nature 392:293–296.

Colbert CM, Magee JC, Hoffman DA, Johnston D (1997) Slow recovery from inactivation of Na^+ channels underlies the activity-dependent attenuation of dendritic action potentials in hippocampal CA1 pyramidal neurons. J Neurosci 17:6512–6521.

Costa PF (1996) The kinetic parameters of sodium currents in maturing acutely isolated rat hippocampal CA1 neurones. Dev Brain Res 91:29–40.

Crill WE (1996) Persistent sodium currents in mammalian central neurons. Annu Rev Physiol 58:349–362.

Cummins TR, Waxman SG (1997) Downregulation of TTX-resistant sodium currents and upregulation of a rapidly repriming TTX-sensitive sodium current in small spinal sensory neurons after nerve injury. J Neurosci 17:3503–3514.

Dib-Hajj SD, Ishikawa K, Cummins TR, Waxman SG (1997) Insertion of a SNS-specific tetrapeptide in S3–S4 linker of D4 accelerates recovery from inactivation of skeletal muscle voltage-gated Na channel μ1 in HEK293 cells. FEBS Lett 416:11–14.

Dib-Hajj SD, Tyrrell L, Black JA, Waxman SG (1998) NaN, a novel

voltage-gated Na channel, is expressed preferentially in peripheral sensory neurons and down-regulated after axotomy. Proc Natl Acad Sci USA 95:8963–8968.

Elliott AA, Elliott JR (1993) Characterization of TTX-sensitive and TTX-resistant sodium currents in small cells from adult rat dorsal root ganglia. J Physiol (Lond) 463:39–56.

Feigenspan A, Gustincich S, Bean BP, Raviola E (1998) Spontaneous activity of solitary dopaminergic cells of the retina. J Neurosci 18:6776–6789.

Felts PA, Yokoyama S, Dib-Hajj S, Black JA, Waxman SG (1997) Sodium channel α-subunit mRNAs I, II, III, NaG, Na6 and hNE (PN1): different expression patterns in developing rat nervous system. Mol Brain Res 45:71–82.

Fern R, Black JA, Ransom BR, Waxman SG (1996) Cd^{2+}-induced injury in CNS white matter. J Neurophysiol 76:3264–3273.

Fleidervish IA, Gutnick MJ (1996) Kinetics of slow inactivation of persistent sodium current in layer V neurons of mouse neocortical slices. J Neurophysiol 76:2125–2130.

Fozzard HA, Hanck DA (1996) Structure and function of voltage-dependent sodium channels: comparison of brain II and cardiac isoforms. Physiol Rev 76:887–926.

Frederickson CJ, Moncrieff DW (1994) Zinc-containing neurons. Biol Signals 3:127–139.

Fukahori M, Itoh M (1990) Effects of dietary zinc status on seizure susceptibility and hippocampal zinc content in the *El* (epilepsy) mouse. Brain Res 529:16–22.

Gabbiani G, Gregory A, Biac D (1967) Cadmium-induced selective lesions of sensory ganglia. J Neuropathol Exp Neurol 26:498–506.

George Jr AL, Komisarof J, Kallen RG, Barchi RL (1992) Primary structure of the adult human skeletal muscle voltage-dependent sodium channel. Ann Neurol 31:131–137.

Gilly WF, Armstrong CM (1984) Threshold channels–a novel type of sodium channel in squid giant axons. Nature 309:449–450.

Howe JR, Ritchie JM (1992) Multiple kinetic components of sodium channel inactivation in rabbit Schwann cells. J Physiol (Lond) 455:529–566.

Izumi H, Mori H, Uchiyama T, Kuwazuru S, Ozima Y, Nakamura I, Taguchi S (1995) Sensitization of nociceptive C-fibers in zinc-deficient rats. Am J Physiol 268:R1423–R1428.

Ji S, George AL, Horn R, Barchi RL (1996) Paramyotonia congenita mutations reveal different roles for segments S3 and S4 of domain D4 in hSkM1 sodium channel gating. J Gen Physiol 107:183–194.

Jung H-Y, Mickus T, Spruston N (1997) Prolonged sodium channel inactivation contributes to dendritic action potential attenuation in hippocampal pyramidal neurons. J Neurosci 17:6639–6646.

Kapoor R, Li YG, Smith KJ (1997) Slow sodium-dependent potential oscillations contribute to ectopic firing in mammalian demyelinated axons. Brain 120:647–652.

Klugbauer N, Lacinova L, Flockerzi V, Hofmann F (1995) Structure and functional expression of a new member of the tetrodotoxin-sensitive voltage-activated sodium channel family from human neuroendocrine cells. EMBO J 14:1084–1090.

Kuo C, Bean BP (1994) Na^+ channels must deactivate to recover from inactivation. Neuron 12:819–829.

Martina M, Jonas P (1997) Functional differences in Na^+ channel gating between fast-spiking interneurones and principal neurones of rat hippocampus. J Physiol (Lond) 505:593–603.

Parri HR, Crunelli V (1998) Sodium current in rat and cat thalamocortical neurons: role of a non-inactivating component in tonic and burst firing. J Neurosci 18:854–867.

Pennartz CMA, Bierlaagh MA, Guersten AMS (1997) Cellular mechanisms underlying spontaneous firing in rat suprachiasmatic nucleus: involvement of a slowly inactivating component of sodium current. J Neurophysiol 78:1811–1825.

Raman IM, Bean BP (1997) Resurgent sodium current and action potential formation in dissociated cerebellar Purkinje neurons. J Neurosci 17:4517–4526.

Raman IM, Sprunger LK, Meisler MH, Bean BP (1997) Altered subthreshold sodium currents and disrupted firing patterns in Purkinje neurons of Scn8a mutant mice. Neuron 19:881–891.

Sakar SN, Adhikari A, Sikdar SK (1995) Kinetic characterization of rat brain type IIA sodium channel α-subunit stably expressed in a somatic cell line. J Physiol (Lond) 488:633–645.

Sangameswaran L, Delgado SG, Fish LM, Koch BD, Jakeman LB, Stewart GR, Sze P, Hunter JC, Eglen RM, Herman RC (1996) Structure and function of a novel voltage-gated tetrodotoxin-resistant sodium channel specific to sensory neurons. J Biol Chem 271:5953–5956.

Sangameswaran L, Fish LM, Koch BD, Rabert DK, Delgado SG, Ilnicka M, Jakeman LB, Novakovic S, Wong K, Sze P, Tzoumaka E, Stewart GR, Herman RC, Eglen RM, Hunter JC (1997) A novel tetrodotoxin-sensitive voltage-gated sodium channel expressed in rat and human dorsal root ganglia. J Biol Chem 272:14805–14809.

Sato K, Iwamasa T, Tsuru T, Takeuchi T (1978) An ultrastructural study of chronic cadmium chloride-induced neuropathy. Acta Neuropathol (Berl) 41:185–190.

Schwindt PC, Crill WE (1995) Amplification of synaptic current by persistent sodium conductance in apical dendrite of neocortical neurons. J Neurophysiol 74:2220–2224.

Smith MR, Goldin AL (1997) Interaction between the sodium channel inactivation linker and domain III S4–S5. Biophys J 73:1885–1895.

Smith RD, Goldin AL (1998) Functional analysis of rat I sodium channel in *Xenopus* oocytes. J Neurosci 18:811–820.

Stafstrom CF, Schwindt PC, Chubb MC, Crill WE (1985) Properties of persistent sodium conductance and calcium conductance of layer V neurons from cat sensorimotor cortex in vitro. J Neurophysiol 53:153–170.

Study RE, Kral MG (1996) Spontaneous action potential activity in isolated dorsal root ganglion neurons from rats with a painful neuropathy. Pain 65:235–249.

Stys PK, Sontheimer H, Ransom BR, Waxman SG (1993) Noninactivating, tetrodotoxin-sensitive Na^+ conductance in rat optic nerve axons. Proc Natl Acad Sci USA 90:6976–6980.

Toledo-Aral JJ, Moss BL, He Z-J, Koszowski AG, Whisenand T, Levinson SR, Wolf JJ, Silos-Santiago I, Halegoua S, Mandel G (1997) Identification of PN1, a predominant voltage-dependent sodium channel expressed principally in peripheral neurons. Proc Natl Acad Sci USA 94:1527–1532.

Vandenberg CA, Bezanilla F (1991) A sodium channel gating model based on single channel, macroscopic and gating currents in the squid giant axon. Biophys J 60:1511–1533.

Westenbroek RE, Merrick DK, Catterall WA (1989) Differential subcellular localization of the R_I and R_{II} Na^+ channel subtypes in central neurons. Neuron 3:695–700.

Wong KL, Klaassen CD (1982) Neurotoxic effects of cadmium in young rats. Toxicol Appl Pharmacol 63:330–337.

Yang N, Ji S, Zhou M, Ptacek LJ, Barchi RL, Horn R, George AL (1994) Sodium channel mutations in paramyotonia congenita exhibit similar biophysical phenotypes *in vitro*. Proc Natl Acad Sci USA 91:12785–12789.